



Structure and Infrastructure Engineering

Maintenance, Management, Life-Cycle Design and Performance

ISSN: (Print) (Online) Journal homepage: <https://www.tandfonline.com/loi/nsie20>

Wavelet-based operating deflection shapes for locating scour-related stiffness losses in multi-span bridges

Eugene J. OBrien, Daniel P. McCrum, Muhammad Arslan Khan & Luke J. Prendergast

To cite this article: Eugene J. OBrien, Daniel P. McCrum, Muhammad Arslan Khan & Luke J. Prendergast (2021): Wavelet-based operating deflection shapes for locating scour-related stiffness losses in multi-span bridges, Structure and Infrastructure Engineering, DOI: [10.1080/15732479.2021.1937235](https://doi.org/10.1080/15732479.2021.1937235)

To link to this article: <https://doi.org/10.1080/15732479.2021.1937235>



© 2021 The Author(s). Published by Informa UK Limited, trading as Taylor & Francis Group



Published online: 12 Jun 2021.



Submit your article to this journal [↗](#)



Article views: 167




View related articles [↗](#)



View Crossmark data [↗](#)

Wavelet-based operating deflection shapes for locating scour-related stiffness losses in multi-span bridges

Eugene J. OBrien^a , Daniel P. McCrum^a , Muhammad Arslan Khan^a  and Luke J. Prendergast^b 

^aSchool of Civil Engineering, University College Dublin, Belfield, Ireland; ^bDepartment of Civil Engineering, Faculty of Engineering, University of Nottingham, Nottingham, UK

ABSTRACT

Scour erosion poses a significant risk to bridge safety worldwide and affects the stiffness of the soil-foundation system, resulting in global changes in the dynamic behavior of the bridges. In this paper, a new approach to detect scour at multiple locations is proposed, using wavelet-based Operating Deflection Shape (ODS) amplitudes. A numerical model of a bridge with four simply supported spans resting on piers is used to test the approach. Scour is modelled as a reduction in vertical foundation stiffness under one or multiple bridge piers. A fleet of passing trucks, modelled as half-car vehicles, are used to excite the bridge to enable structural accelerations be calculated at each support. The approach is shown to be effective with acceleration measurements at each support location in a multi-span bridge. Using a fleet of passing vehicles, the temporal accelerations measured at each support are averaged and transformed into the frequency-spatial domain, in order to estimate the wavelet-based ODS for a given scour case. A damage indicator is postulated based on differences between the ODS of healthy and scoured bridge cases. The damage indicator enables visual identification of the location of scoured piers considering a range of natural frequencies of the system.

ARTICLE HISTORY

Received 12 December 2020
Revised 26 February 2021
Accepted 21 March 2021

KEYWORDS

Bridge damage; operational deflection shapes; scour erosion; structural health monitoring; vehicle-bridge interaction; wavelet analysis

1. Introduction

Bridge scour is the term used to describe the washing away of soil (erosion) near bridge foundations due to hydraulic action (Hamill, 1999). Scour is responsible for a majority of bridge failures worldwide (Maddison, 2012; Melville & Coleman, 2000; Wardhana & Hadipriono, 2003) and can cause significant economic losses and travel disruptions (Lagasse et al., 1995). Scour reduces the elevation of the soil surface profile in the vicinity of bridge foundations, which affects the capacity and stiffness of these systems (Malekjafarian et al., 2020). The detection of scour and scour-related damage in structures is a problem that has received increasing research attention in recent years (Bao et al., 2017; Bao & Liu, 2017; Fitzgerald et al., 2019a, 2019b; Foti & Sabia, 2011; Giordano et al., 2020; Ju, 2013; Kong & Cai, 2016; Li et al., 2020; Malekjafarian et al., 2020; Prendergast et al., 2016a, 2016b, 2017; Xiong et al., 2018).

The most popular way to detect and monitor scour occurrence remains visual inspections by asset agencies, involving divers inspecting foundation condition, often using rating-based metrics for scour severity. Though popular, this approach is subjective, costly, labour-intensive, and critically cannot be undertaken when rivers are flooded, when scour risk is likely to be highest. Other approaches involve the use of scour hole monitoring instrumentation

and sensors (Fisher et al., 2013; Prendergast & Gavin, 2014), the common drawback being that these systems focus on scour hole magnitude measurement, and not the effect the scour hole has on the structure.

Many damage detection approaches do not address the issue of when intervention measures might be required to contain the problem. In the context of scour, this is a major challenge due to the nonlinear relationship between scour depth and the resulting variations in stiffness and capacity that might arise. However, in these approaches, should stiffness loss be detected, then a visual inspection could be triggered to prompt asset managers to take a closer look. There have been developments in recent years in the area of quantifying the value of information to determine how decisions can be made related to intervention measures—see for example, Giordano et al. (2020).

Emerging approaches involve the use of vibration sensors, particularly accelerometers, to measure the structural responses (direct) or the traversing vehicle responses (indirect) to detect scour-related damage. These methods aim to detect any changes in structural behaviour as a result of the stiffness loss caused by scour, by monitoring changes in bridge modal parameters, such as natural frequencies (Bao et al., 2017; Bao & Liu, 2017; Foti & Sabia, 2011; Ju, 2013; Malekjafarian et al., 2020; Prendergast et al., 2013; Prendergast & Gavin, 2014), mode shapes (Bao & Liu, 2017;

Fitzgerald et al., 2019a; Malekjafarian et al., 2020; Prendergast & Gavin, 2014) and damping (Buckley et al., 2018). Due to the tendency for inaccuracies in the measurement of damping (Xiang et al., 2013), methods based on natural frequency and mode shape related changes have received more attention for scour damage detection.

While several of these approaches have shown potential success at detecting the presence of scour at one pier location of a bridge (Malekjafarian et al., 2020; Prendergast et al., 2016a, 2016b), the ability to detect scour at multiple locations remains a challenge. Some authors have attempted to remedy this: for example, Prendergast et al., (2017) proposed a method for detecting the location of scour in a two-span integral bridge by analysing higher order modal frequencies and correlating the frequency change measured in certain modes with the location of scour. The method showed potential success at detecting scour location in a two-span integral bridge; however, expansion of the approach to multi-span bridge systems remains a challenge.

Operating deflection shapes (ODS) are a commonly used technique to visualize vibration patterns in structures under operating conditions. These can provide a visualization of the deflection magnitude at various points of a structure as a function of frequency (Richardson, 1997; Schwarz & Richardson, 1999; Vold et al., 2000). ODS-based damage detection approaches have been proposed for crack detection in structures (Bai et al., 2014; Xiang et al., 2013) and machinery (Zhang et al., 2013a, 2013b) and can assist in identifying anomalies in geometric features of structures. In the simplest approach, ODS can be measured using a fast Fourier transform (FFT) applied to acceleration signals from any location, or the Auto Power Spectrum (APS) can be calculated by multiplying the complex FFT spectrum by its complex conjugate.

Although APS-based ODS exhibit high resilience against signal noise, the phase values of the ODS are not preserved. Traditionally, ODS are measured using a multi-channel signal analyser that includes a reference-input (excitation) and multiple output signals. The output signals are compared to the reference signal to obtain frequency response functions (FRF), which provide the magnitude and phase of the ODS in the frequency domain (Schwarz & Richardson, 1999; Vold et al., 2000). However, in the case of real bridges, it is difficult to measure the forcing function caused by traversing random vehicles, and only output acceleration signals at multiple locations can typically be measured.

When excitation forces are unknown, transmissibility measurements can be used, which consider a single reference output signal and multiple measured output signals to calculate ODS relative to the reference point (Schwarz & Richardson, 2004; Vold et al., 2000). Although the magnitude and phase of the ODS are preserved using this approach, it does not generate peaks at resonance frequencies; rather a plateau occurs at the structural natural frequencies (Schwarz et al., 2019). To resolve this issue, Schwarz & Richardson (2004) propose a combined ODS-FRF approach that replaces a cross spectrum (i.e. relationship between reference and measurement signals) with a

square root of the APS magnitude. However, by doing this, the results do not account for load variations and the ODS functions must be rescaled between measurement sets to adjust for these variations (Schwarz & Richardson, 2004).

ODS-based damage detection techniques have been researched in the past for various different structures, including machines (Reilly, 2011), single-span bridges (Cao et al., 2017; de Siqueira & Nogueira, 2001; Xiang et al., 2013; Xu et al., 2013; Yoon et al., 2010; Zhang et al., 2013b), wind turbines (Zhang et al., 2013a), and gearboxes (Gade et al., 2009). Most of the proposed approaches aim to detect local damage such as cracks or debonding (Cao et al., 2017) using either ODS directly, or using ODS curvature (CODS) (Cao et al., 2017; Zhang et al., 2013b). In recent years, the use of wavelet transforms to estimate ODS and CODS has been investigated for crack detection in beam-like structures (Cao et al., 2017; Fitzgerald et al., 2019b; Hera & Hou, 2004; Hou et al., 2000; Xu et al., 2013; Zhu & Law, 2006).

The main advantage of the continuous wavelet transform (CWT) is its ability to provide dynamic information simultaneously in the frequency and time domains with adaptive windows. Wavelet transforms contain local singularity information, which enables the detection of damage location and severity (Zhu & Law, 2006). ODS contain the contributions from all operating modes at any frequency (Schwarz & Richardson, 1999) and can be analysed using a wavelet transform. In this way, ODS can be used to locate damage in the affected structure. However, it should be noted that in the process of obtaining wavelet transforms, the so-called boundary distortion phenomenon (Asnaashari & Sinha, 2014) occurs due to the finite length of the signal near boundaries. This phenomenon influences the ability of wavelets to detect singularities, or damage, occurring near the bridge boundaries.

In this paper, a novel approach to detect the presence and location of scour damage affecting a multi-span bridge structure is proposed using wavelet-based ODS, where the excitation comes from forced vibrations due to traversing vehicles. ODS are calculated using the APS of the signals' wavelet transforms, which is investigated over a range of frequencies for both healthy (undamaged) and scoured bridge conditions. Bridge accelerations calculated at each support due to the actions of traversing vehicles are analysed. To mitigate the effects of varying vehicle velocities and masses on the resulting bridge accelerations, an average bridge acceleration is obtained at each point of the bridge from a statistical population of traversing vehicles (by converting the time-varying bridge response to a spatially-varying response along the structure). This approach is tested using a four-span numerical model of a bridge (Cantero et al., 2010; González, 2010), where piers are considered as sprung masses (Fitzgerald et al., 2019a, 2019b), and foundations are modelled using vertical springs and dashpots for foundation stiffness and damping, respectively (Adhikary et al., 2014; Buckley et al., 2018; Ju, 2013; Mylonakis et al., 2006).

In this work, five 'accelerometers' (node points in the numerical model) are considered to be present at the five

pier supports. A population of 2-axle vehicles, developed from a database of measured Weigh-In-Motion (WIM) data from a field site, is used to characterize the properties of the modelled half-car vehicles. A class 'A' road profile is included on the bridge (Tyan et al., 2009). Wavelet-based ODS amplitudes of the spatially-averaged accelerations are measured by calculating the APS of the wavelet energy coefficients for both healthy and scoured bridge conditions, where scour is modelled as a loss of foundation stiffness at various supports of the bridge. The difference between healthy and scoured wavelet-based ODS amplitudes is considered as a damage indicator and enables the detection of scour at both a single location and multiple locations. This approach can determine if damage has occurred and the location of the damaged pier without quantifying the magnitude of damage. The numerical results demonstrate the potential effectiveness of wavelet-based ODS at detecting the presence and location of scour at multiple locations on a bridge.

2. Vehicle-bridge interaction model

2.1. Bridge model

A four-span single-lane bridge (see Figure 1) is modelled in MATLAB with 1D finite element Euler-Bernoulli beam elements (González, 2010; Kwon & Bang, 2000). Each span is modelled using twenty 1 m long elements, each with four degrees of freedom (DOF) (Kwon & Bang, 2000). Spans are considered as simply-supported and connected on hinged supports, which rest on deformable piers, each modelled as a single DOF sprung mass (with mass $m_{su,i}$ and stiffness, $k_{su,i}$ for the i th support, respectively). The supports are assumed to rest on shallow pad foundations, which are modelled using a foundation stiffness $k_{f,i}$ and soil damping dashpot $C_{f,i}$ ($i = 1, 2, \dots, N_p$), where N_p is the number of supports.

The foundation stiffness and damping are derived to correspond to a 4 m × 2 m foundation (in plan) with no side wall, embedded to a depth of 0.5 m in a medium dense sand deposit (Fitzgerald et al., 2019b). Stiffness and damping are derived using the following expressions (Mylonakis et al., 2006):

$$k_{f,i} = \frac{2GB}{1-\nu} \left[1.53 \left(\frac{L}{4B} \right)^{0.75} + 0.73 \right] \times \left[1 + \left(\frac{1}{21} \right) \left(\frac{d_{emb}}{B} \right) \left(1 + 1.3 \times \frac{L}{4B} \right) \right] \quad (1)$$

$$C_{f,i} = \left[2 \times \bar{k} \times \frac{k_f \beta}{\omega_s} \right] + (\rho V_{LA} A_b) \bar{c}_z \quad (2)$$

where G is the soil shear modulus (kPa), ν is Poisson's ratio, L , B and d_{emb} are the foundation length (m), width (m) and embedded depth (m), respectively. The parameters \bar{k} , β and ω_s are the dynamic stiffness for the embedded foundation, hysteretic dynamic coefficient of 7%, and the ground excitation frequency (Mylonakis et al., 2006), respectively.

The parameters ρ , V_{LA} and A_b are soil density, Lysmer's analog velocity and cross-sectional area of the foundation, respectively. \bar{c}_z is a radiation damping coefficient that can be estimated using graphical methods and equations in (Mylonakis et al., 2006). Further details of Eqs. (1) and (2) can be found in (Mylonakis et al., 2006). The shear modulus, G is calculated from the soil elastic modulus, E_s , using the expression $G = E_s / (2 \cdot (1 + \nu))$, where $E_s = 100,000$ kPa for medium-dense sand (Prendergast & Gavin, 2016a). Equations (1) and (2) are semi-empirical and more information on similar expressions is available in (Mylonakis et al., 2006; Pais & Kausel, 1988). This bridge model simulates a simple soil-structure interaction system and does not account for asymmetric behaviour and non-linear changes in soil properties that may occur due to scour. The geometric and material properties of the bridge and foundation are provided in Table 1.

The bridge contains a road surface profile with a class 'A' roughness classification and geometric spatial mean of 16×10^{-6} m³/cycle (Tyan et al., 2009) generated according to the ISO standard (ISO, 1995). An approach length of 100 m is modelled so that the initial conditions of the vehicle are more realistic when it enters the bridge. The dynamic response can be calculated by solving the equation of motion:

$$M_b \ddot{y}_b + C_b \dot{y}_b + K_b y_b = f_{int} \quad (3)$$

where M_b , C_b and K_b are bridge mass, damping and stiffness matrices, respectively, and, \ddot{y}_b , \dot{y}_b and y_b are the vectors of bridge accelerations, velocities and displacements for each DOF, respectively. The vector f_{int} represents the interaction forces between the bridge and the vehicle (González, 2010) in a vehicle-bridge interaction system.

2.2. Vehicle model

The vehicle is modelled as a dynamic sub-system that traverses the bridge. A half-car 2-axle vehicle, shown in Figure 2, is modelled (Cantero et al., 2010; Cebon, 1999). The vehicle has four DOFs, a body mass translation (y_s) and pitch (θ), and two axle mass translations ($y_{u,i}$). The axles have masses $m_{u,1}$ and $m_{u,2}$, respectively, and springs with linear stiffness ($k_{s,i}$) and viscous damping coefficient ($C_{s,i}$) connecting them to the body mass (m_s). The vehicle contacts the road surface through tire springs with linear stiffness ($k_{t,i}$) (Cantero et al., 2010). Vehicle properties, e.g., unsprung (axle) masses, suspension and tire stiffnesses, etc., are taken from the literature and are presented in Table 2 (Cantero et al., 2010; Cebon, 1999; Keenahan et al., 2014). The Gross Vehicle Weight (GVW) of each half-car is represented as a sum of axle and body masses.

For each simulation, the GVW and the vehicle velocity are chosen using WIM data from Maryland (part of the U.S. Federal Highway Administration's Long-Term Pavement Performance database) (Walker et al., 2012; Walker & Cebon, 2012), to approximate the nature of real traffic. From the WIM database, the data of 2-axle vehicles,

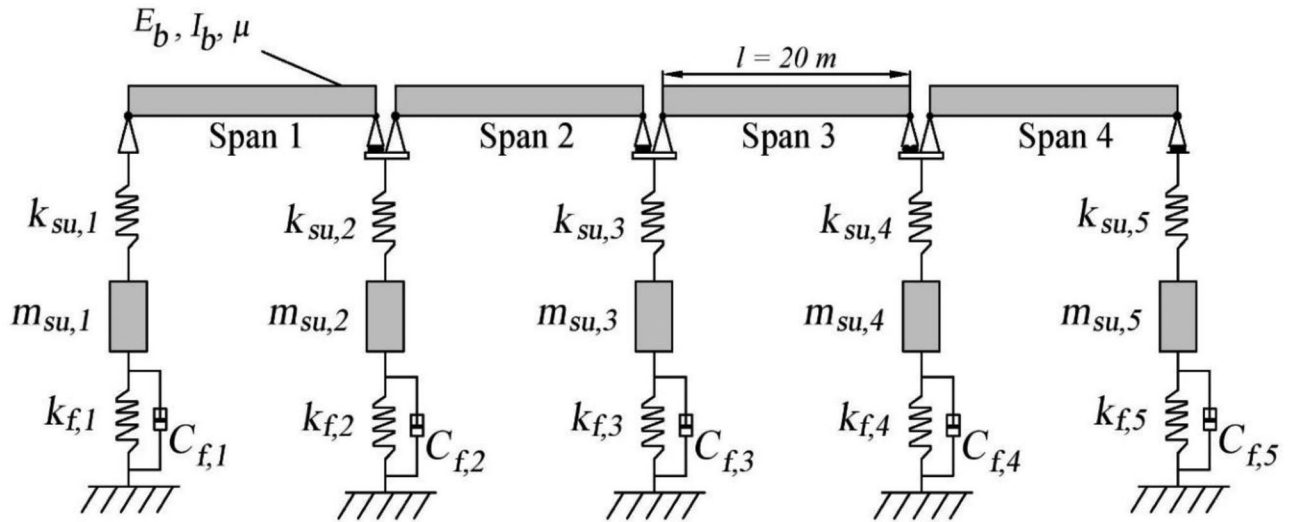


Figure 1. Schematic of the modelled bridge.

Table 1. Geometric and material properties of the bridge model.

Bridge property	Notation	Value
Deck width	b	4 m
Elastic modulus of deck	E	35×10^9 N/m ²
2nd moment of area	I	0.33 m ⁴
Mass per unit length	μ	9600 kg/m
Pier length	l_{pier}	7 m
Pier width	b_{pier}	2.5 m
Pier depth	d_{pier}	1 m
Pier stiffness	$k_{su,i}$	12.50×10^9 N/m
Foundation spring stiffness	$k_{f,i}$	401.22×10^6 N/m
Foundation damping coefficient	$C_{f,i}$	276.75×10^3 Ns/m

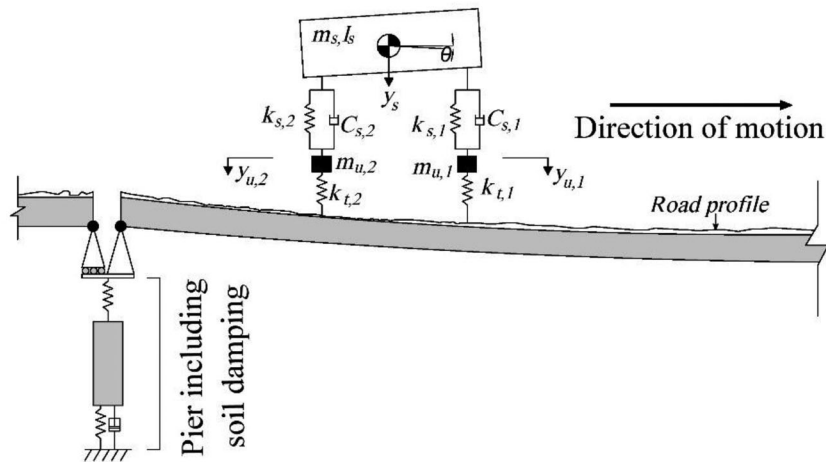


Figure 2. Half-car model on a segment of the bridge (in deflected state), with road profile.

having axle spacings between 5 m and 7 m, is extracted that provides a population of over 169,000 GVWs and velocities, recorded over a period of 8 years. For each simulation run, one vehicle is considered traversing the bridge and this is repeated 1000 times with the axle weights and the velocities for each traversing vehicle extracted from a random location in the database.

The equation of motion for the vehicle is formulated by establishing equilibrium of forces and moments acting on the vehicle DOFs to derive the mass, M_v , damping C_v and stiffness, K_v matrices, respectively:

$$M_v \ddot{y}_v + C_v \dot{y}_v + K_v y_v = f_v \quad (4)$$

where \ddot{y}_v , \dot{y}_v and y_v are the vectors of vehicle accelerations, velocities and displacements, respectively. The vector, f_v represents the time-varying interaction forces applied to the vehicle DOFs, which is a function of the road profile and the bridge displacements.

Dynamic interaction is considered by coupling the vehicle and bridge systems (González, 2010) to form a global equation of motion:

$$M_g \ddot{u} + C_g \dot{u} + K_g u = F \quad (5)$$

Table 2. Properties of the half-car model (Cantero et al., 2010).

Vehicle property	Notation	Value
Axle masses	$m_{u,1}$	750 kg
	$m_{u,2}$	1100 kg
Tire stiffnesses	$k_{t,1}$	1.75×10^6 N/m
	$k_{t,2}$	3.5×10^6 N/m
Suspension stiffnesses	$k_{s,1}$	0.5×10^6 N/m
	$k_{s,2}$	1.0×10^6 N/m
Suspension damping	$C_{s,1}$	1.0×10^4 Ns/m
	$C_{s,2}$	15×10^3 Ns/m

where M_g and C_g are the coupled mass and damping matrices, respectively. The time-varying coupled stiffness matrix, K_g , is dependent on the static displacements of the bridge due to the actions of the traversing vehicle. F represents the system force matrix, and \ddot{u} , \dot{u} and u are the vectors of accelerations, velocities, and displacements of the global coupled system, respectively. Equation (5) is solved in MATLAB using the Wilson-Theta integration scheme (Tedesco et al., 2000), ensuring unconditional stability. A sampling frequency (f_s) of 200 Hz is used in the simulation of bridge accelerations, which vary with time based on the position of the passing vehicle.

3. Effect of scour on bridge modal properties

The erosion of soil from around and under bridge foundations changes the stiffness and strength of these systems. For shallow pad foundations, the combined action of lowering soil elevation and potential undermining has the double effect of changing the overburden-dependent stiffness and altering the soil-foundation contact area, causing an increase in soil strains and subsequently a reduction in vertical stiffness. Recent experimental investigations have revealed the overburden-dependency of soil stiffness for differently shaped scour holes around laterally-loaded pile foundations (Chortis et al., 2020; Li et al., 2020).

Many previous works have focused on scour effects on piled bridges, where the scour-related stiffness reduction mechanism affects the lateral stiffness and capacity of piled foundations (Bao et al., 2019; Bao & Liu, 2020; Elsaid & Seracino, 2014; Foti & Sabia, 2011; Klinga & Alipour, 2015; Prendergast et al., 2016, 2017; Shirgir et al., 2016). In the present work, the focus is on bridges with shallow foundations, where the vertical stiffness is affected by scour undermining the foundation, a mechanism that has received much less attention in previous literature.

The overall damping in the bridge model is considered by the Rayleigh formulation, which is mass and stiffness proportional, so there will be some change in damping due to scour. However, in this paper, the actual specified soil damping remains unchanged before and after scour in the modelling. Additionally, water-added mass effects may reduce the natural frequencies of the system. However, this effect is difficult to quantify and tends to be ignored in bridge natural frequency analysis (Ju, 2013). As it is the relative difference in the dynamic behavior between scoured and unscoured conditions that is of interest, the influence of

water-added mass is not considered in the modelling conducted.

Stiffness losses under scour are modelled in this paper by altering the foundation stiffness values calculated using Eq. (1). Two scour cases are considered: 25% and 45% reduction in foundation stiffness (relative to Eq. (1) values) at piers, which are assumed to occur by the combined reduction in soil shear modulus (Oztoprak & Bolton, 2013) and foundation undermining, changing the soil-foundation contact area. Though seemingly severe reductions in stiffness, these are actually calculated assuming relatively minor changes in soil shear modulus and foundation undermining (Khan et al., 2021).

Figure 3 illustrates the percentage change in natural frequency of a number of modes of the bridge relative to the healthy (undamaged) condition as a result of scour-related stiffness reduction at various supports. Figure 3(a) shows the percentage change of each modal frequency relative to the healthy case for stiffness reductions of 25%, and 45% at the left-hand abutment (Support 1). Figure 3(b)–(e) shows the same data but for scour-related stiffness reductions of 25% and 45% at Supports 2, 3, 4 and 5, respectively (see Figure 1 for bridge schematic). Figure 3(a)–(e) each corresponds to a single scour location at 1st to 5th support, respectively. Table A1 in the Appendix of the paper shows the absolute frequencies for a range of scour cases and modes of vibration (the data shown in Figure 3).

This analysis highlights which modes of the structure exhibit sensitivity to scour at certain supports, and is similar to the analysis in Prendergast et al. (2017), which was applied to integral bridges. It can be seen that different combinations of modes are sensitive to scour at different locations but most of the sensitivity is in Modes 5 to 8 for the current bridge. It should be mentioned that small changes in frequencies and mode shapes due to scour might be overshadowed by changes in bridge dynamic properties occurring as a result of environmental effects (OBrien et al., 2020).

To assist in mitigating this effect, a statistical approach is proposed in this paper which can potentially mitigate against environmental influences overshadowing the effects of damage. The inherent assumption is that data collection is undertaken 24 hours per day, every time that a heavy vehicle passes. It should be noted, however, that variability in environmental effects is not explicitly modelled in the present analysis, and further investigation would be required to determine its influence. It should also be noted that an attempt to identify scour at other piers based on the response of a given pier did not yield consistent or satisfactory results. Therefore, a sensor is required at each pier for which scour information is desired.

Based on the analysis in Figure 3, which shows that multiple modes are influenced simultaneously by scour at various locations, an approach that analyses information relating to a range of modes simultaneously is therefore of potential interest for scour detection. ODS provide an indication of the magnitude of bridge motion at any

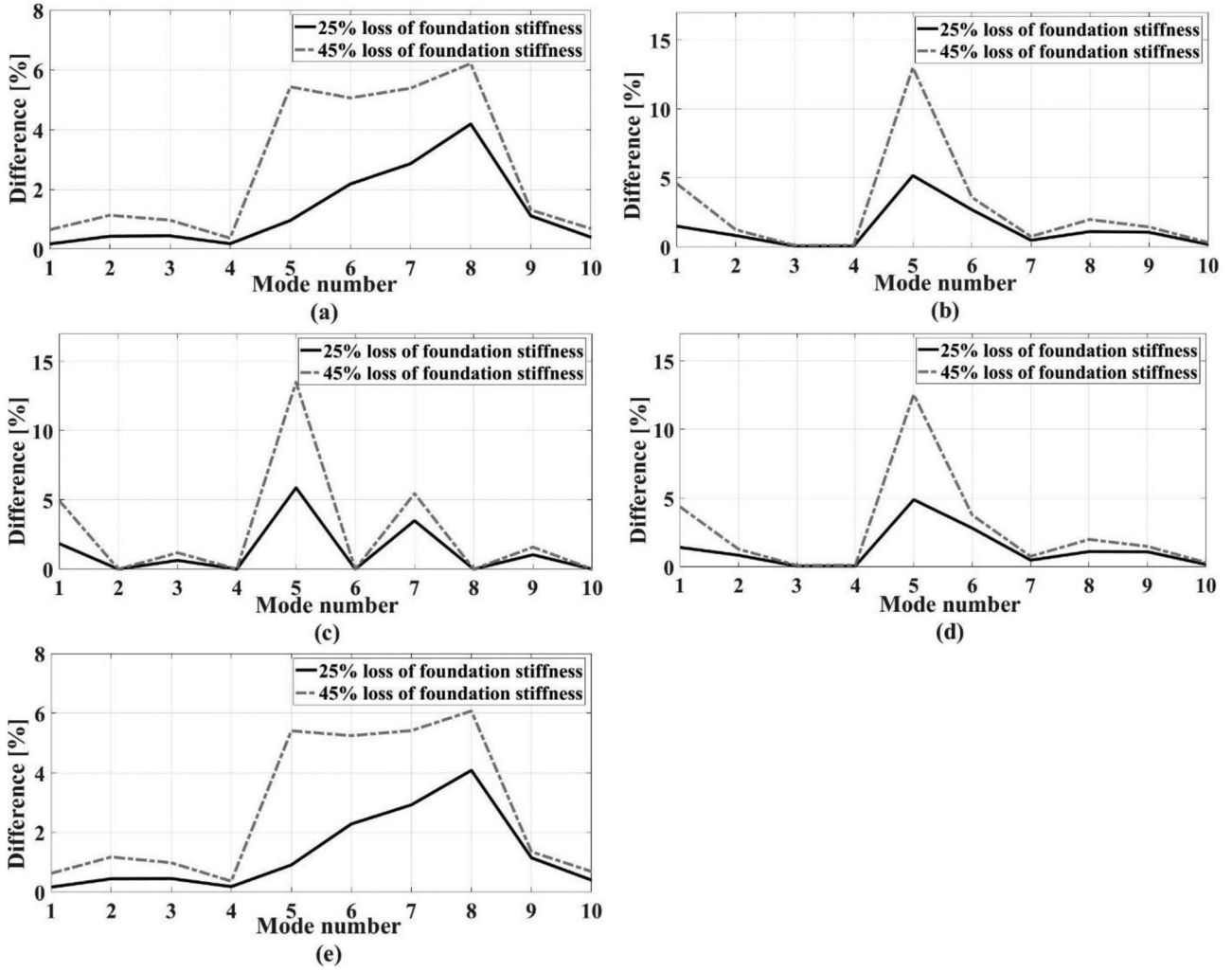


Figure 3. Difference between healthy and scoured bridge natural frequencies when scour is at: (a) left abutment (Support 1); (b) Support 2; (c) Support 3; (d) Support 4; and (e) right abutment (Support 5).

frequency and allow an assessment of the behaviour over a range of frequencies. This is particularly appropriate for multi-span bridges of the type considered in the present work, since many of the modes are closely-spaced therefore identifying changes in individual modes is challenging.

4. Wavelet-based ODS concept for scour detection

In this paper, ODS are analysed using a Continuous Wavelet Transform (CWT) of the acceleration data measured simultaneously at the five bridge supports under the actions of passing vehicles. CWT is a well-known signal processing tool (Teolis & Benedetto, 1998) that can identify the temporal variation in the frequencies of a signal by comparing the responses to the properties of a mother wavelet. Time localization is an important criterion for this approach. For that reason, the Morlet Wavelet, adopted in previous damage detection approaches (Taha et al., 2006), is used in the present work because it provides an appropriate balance between time and frequency resolution, and facilitates time localization (McGetrick & Kim, 2013, 2014). It can be expressed as:

$$\psi(x) = \frac{1}{\sqrt{\pi F_b}} e^{j2\pi F_c x - x^2/F_b} \quad (6)$$

where F_b is a bandwidth parameter, defined as the variance of the Fourier transform of the wavelet, and F_c is the central frequency of the wavelet (Tedesco et al., 2000).

The Morlet generates a complex-valued wavelet which can be expressed as:

$$W_f(s, u) = \frac{1}{\sqrt{s}} \int_{-\infty}^{\infty} f(x) \psi^* \left(\frac{x-u}{s} \right) dx \quad (7)$$

where $W_f(s, u)$ denotes the complex CWT coefficient of a signal $f(x)$ with s and u being the scale and translation parameters, respectively. $\psi^*(x)$ denotes the complex conjugate of $\psi(x)$. Wavelet-based ODS magnitudes are calculated by multiplying CWT coefficients by their complex conjugates. Similar to the APS (Schwarz & Richardson, 1999), Wavelet-based ODS do not preserve phase information.

Bridge accelerations under the action of traversing vehicles with Gross Vehicle Weights (GVW) of 8.8 t and speed of 90 km/h, which correspond to the mean values from the 2-axle WIM data, are calculated in this section using a sampling frequency of 200 Hz. Figure 4 illustrates the Wavelet-derived ODS magnitudes at the three interior

supports (piers) (Supports 2–4) calculated using the accelerations measured at these locations, i.e. finite element nodes at the interior supports representing vertical movement of piers. In this paper, the abutment supports (Supports 1 and 5) are excluded from the analysis because they are assumed to be out of the water and not prone to scour. The frequency range of interest is determined to be between 0 Hz and 14 Hz, which covers the spectrum of the first nine bridge natural frequencies—see Table 3.

Since damage location is of interest, the time-domain data is represented in the spatial domain, using the vehicle velocity to transform time to vehicle distance along the bridge. The shading for each plot in Figure 4 is consistent across all plots, i.e. the data is plotted on the same scale, with yellow colour being indicative of positive maximum and dark blue of negative minimum. The vertical dashed lines in Figure 4 indicate the location of sensors used to derive the information in the given plot, and the corresponding support where the sensor is located.

In Figure 4(a), it can be seen that a higher magnitude of ODS occurs for frequencies in the 9–12 Hz range (Modes 5–7) when the vehicle crosses over the support where the sensor is located. This high-intensity (light-coloured) band shifts to the right when the sensor is at the 40 m point (Figure 4b) and further to the right when the sensor is at the 60 m point (Figure 4c). A less intense light-coloured band occurs in the vicinity of the bridge first natural frequency, at approximately 4 Hz. This also shifts with sensor location, but the effect is less pronounced than for the higher frequencies. Since the wavelet-based approaches may encounter edge effects in the response, the frequency range analysed in Figure 4 is extended in Figure 5, for the same vehicle properties.

The edge effects can be seen in Figure 5(a)–(c) in the form of vertical contour lines, near or at the sensor locations in the frequency range from 20 Hz to 65 Hz. In this paper, the frequency range between 0 Hz and 14 Hz is used for which the edge effects are seen to not be as significant, as compared to the ODS magnitudes of the bridge frequencies (see Figure 5). For this reason, the proposed approach assesses the wavelet-based ODS without the need for removing/reducing edge effects in the response. The analysis in this section is for the healthy bridge case, i.e. no scour damage has been introduced into the model. The results show that certain frequencies associated with the structure are excited at a given sensor location when the vehicle traverses the point of the bridge where the sensor is located.

4.1. Effect of vehicle properties on ODS

One of the great challenges in Structural Health Monitoring is that the main source of dynamic excitation comes from vehicles, which can have a wide range of velocities and masses. This section investigates the sensitivity of the wavelet-derived ODS to vehicle variability. Velocity of the vehicle can influence measured accelerations arising within the vehicle and on the bridge being traversed by changing the dynamic interaction between the two sub-systems (M1zrak

& Esen, 2015; OBrien et al., 2020). The effect of vehicle velocity can be to augment or diminish the corresponding bridge accelerations, depending on whether there is constructive or destructive interference between the vehicle and the bridge vibrations (OBrien et al., 2020).

Figure 6 investigates the influence of changing the vehicle velocity relative to the data presented in Figure 4. The mass of the vehicle is kept constant at 8.8 t but a higher velocity of 100 km/h is used, which is approximately equal to the mean velocity (= 90 km/h) + one standard deviation (= 9.9 km/h) from the 2-axle WIM data used previously. It can be seen in Figure 6 that lower frequencies in a range of 3–5 Hz (corresponding to the first 4 natural frequencies of the bridge) are excited more as compared to Figure 4. Similarly, the higher range frequencies (7–14 Hz) in Figure 6 are not excited as much as compared to Figure 4. This brief analysis suggests that the change in vehicle velocity can impact the ODS at certain frequencies by increasing its magnitude (by constructive interference between vehicle and bridge vibrations) and vice versa (by destructive interference between vehicle and bridge vibrations).

Bridge accelerations may also be affected by changes in vehicle GVW (OBrien et al., 2020; Sekiya et al., 2018) so this is investigated briefly herein. The influence of an increase in GVW by 1.8 t (approximately one standard deviation of the 2-axle WIM data), is shown in Figure 7. The velocity is maintained the same as that assumed for Figure 4 at 90 km/h. As compared to Figure 4, it can be seen in Figure 7 that the overall trend in the results is broadly unaffected by the change in the vehicle mass. This is not surprising even though the effect of mass is to alter the vehicle dynamic properties since the main change in vehicle-bridge interaction would occur due to changes in velocity influencing the constructive/destructive interference, as evidenced in Figure 6.

The combined influence of changing mass and velocity is investigated in Figure 8. The vehicle mass and velocity are increased by 1.8 t and 10 km/h, respectively, and the wavelet-based ODS are illustrated in Figure 8. It can be seen in this figure that the results are quite similar to the one showing the influence of velocity (Figure 6), which again suggests that the magnitudes in these plots are affected by velocity but not so much by mass. This brief analysis highlights the importance of interaction effects between the pseudo-frequencies associated with traversing vehicles and bridges, which dominate the spectra as compared to changes in mass which have little influence. In order to minimize the effect of this interaction, this paper proposes a statistical approach to detect scour.

5. Damage indicator for scour detection

In this paper, a statistical approach is proposed for detecting scour location that combines data from a fleet of typical vehicles with a wide range of velocities and masses. A fleet of 1000 vehicles is considered to cross the bridge with the GVW and velocity chosen randomly from the 2-axle WIM data for each run to obtain statistical bridge accelerations. A

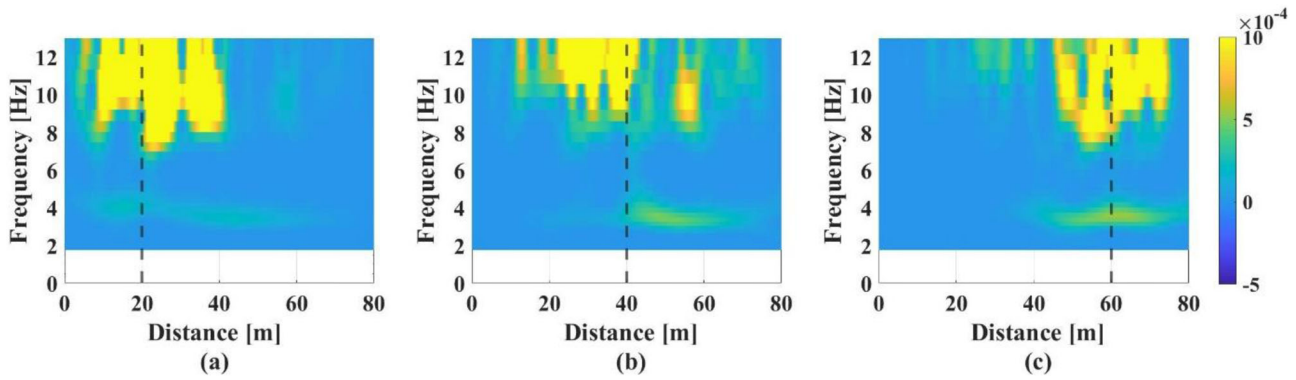


Figure 4. Wavelet-based ODS in frequency and distance domain for healthy bridge excited by vehicle with GVW = 8.8 t and velocity = 90 km/h with sensor at: (a) Support 2; (b) Support 3; and (c) Support 4. Vertical dashed line indicates the location of sensor in each plot.

Table 3. First nine bridge natural frequencies.

Mode number	1	2	3	4	5	6	7	8	9
Frequency/Hz	3.81	3.93	4.10	4.26	9.50	10.29	11.46	12.95	13.47

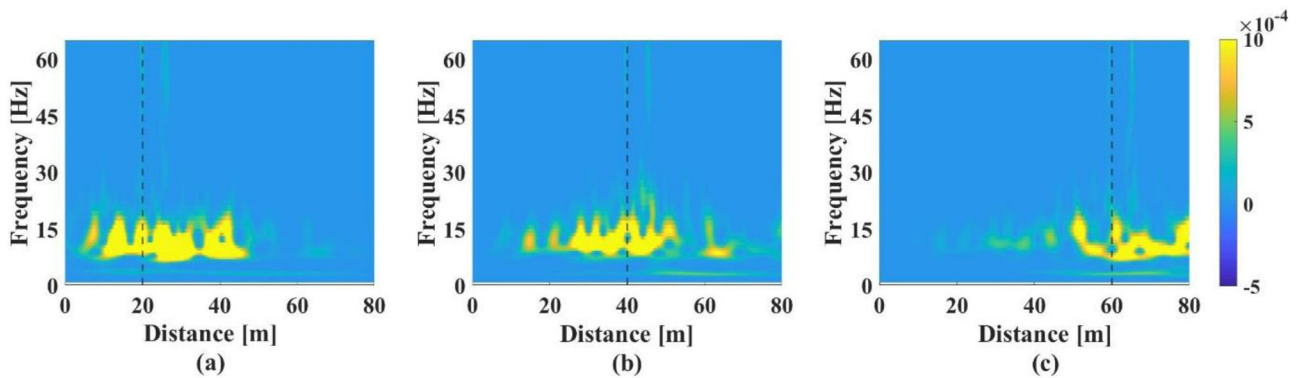


Figure 5. Wavelet-based ODS in frequency (extended range) and distance domain for healthy bridge excited by vehicle with GVW = 8.8 t and velocity = 90 km/h with sensor at: (a) Support 2; (b) Support 3; and (c) Support 4. Vertical dashed line indicates the location of sensor.

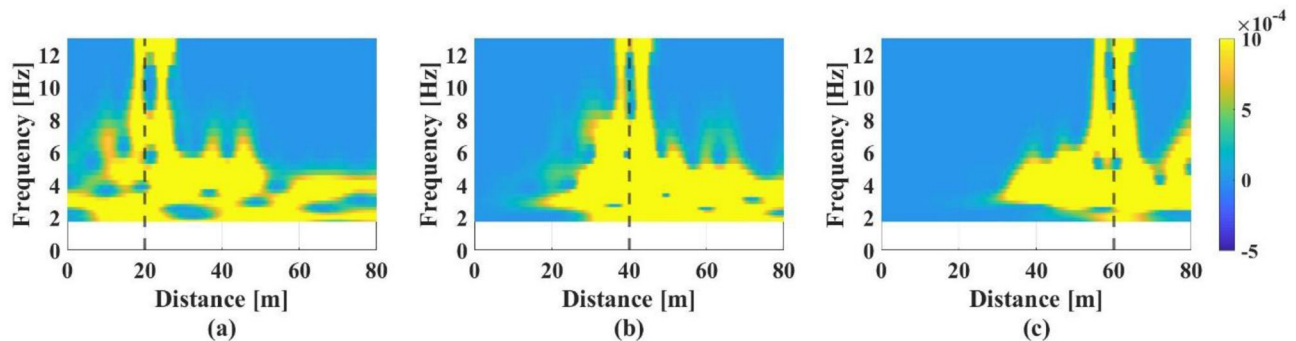


Figure 6. Wavelet-based ODS plot in frequency and distance domain for healthy bridge excited by vehicle with GVW = 8.8 t and velocity = 100 km/h with sensor at: (a) Support 2; (b) Support 3; and (c) Support 4. Vertical dashed line indicates location of sensor in each plot.

fleet is modelled consisting of 1000 separate vehicle crossing events with variable weights and velocities. This results in a statistical population of responses.

In order to ensure the signals obtained are more representative of what would be expected from real sensors, noise, specified using normally distributed randomly generated noise amplitudes—with a mean of zero and standard deviation ranging between 3.5% and 8.5% of the maximum absolute acceleration amplitude, depending on the gross vehicle weights (Keenahan et al., 2014; Khan et al., 2021)—

is added to the clean accelerations. These percentages are based on a sample of field acceleration measurements and signal-to-noise ratio from accelerations due to traversing vehicles with different gross vehicle weights. The simulated acceleration signals, due to an 8.8 t GVW vehicle traveling at 90 km/h speed, with and without noise, are shown in Figure 9.

The time-domain acceleration signal from each run is converted to the spatial-domain to correspond to the location on the bridge where the vehicle is located at a given

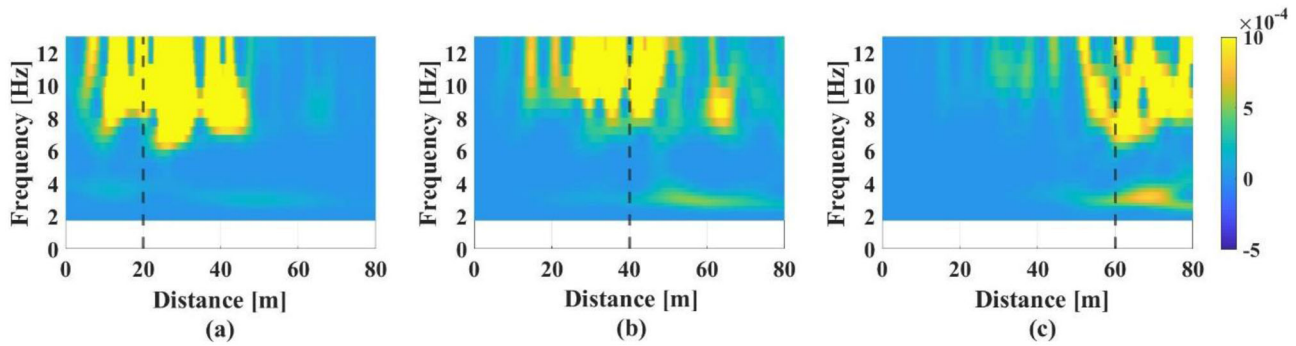


Figure 7. Wavelet-based ODS plot in frequency and distance domain for healthy bridge excited by vehicle with GVW = 10.6 t and velocity = 90 km/h with sensor at: (a) Support 2; (b) Support 3; and (c) Support 4. Vertical dashed line indicates location of sensor in each plot.

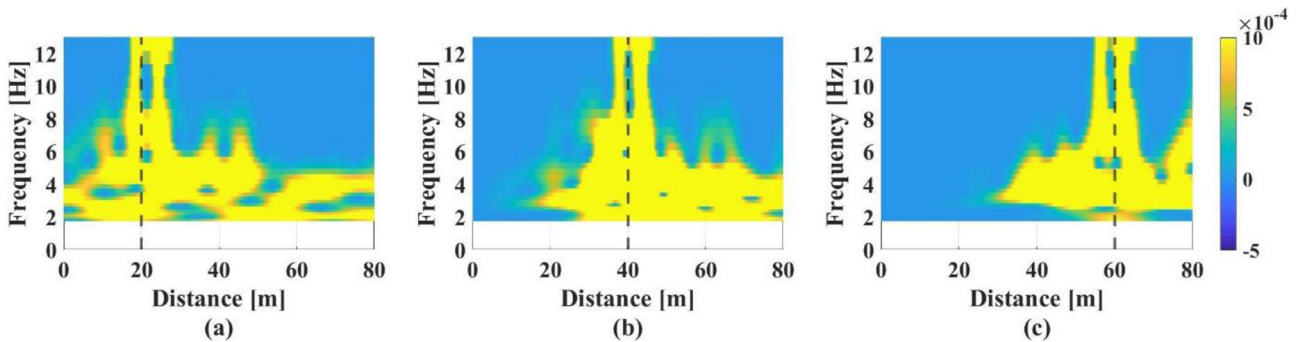


Figure 8. Wavelet-based ODS plot in frequency and distance domain for healthy bridge excited by vehicle with GVW = 10.6 t and velocity = 100 km/h with sensor at: (a) Support 2; (b) Support 3; and (c) Support 4. Vertical dashed line indicates location of sensor in each plot.

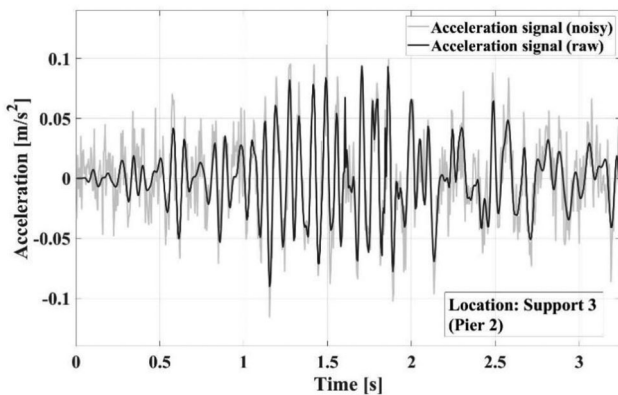


Figure 9. Acceleration signal at Support 3 (pier 2) due to a traversing half-car, with and without noise.

time increment. The resulting spatial acceleration signals are then averaged for the fleet of 1000 vehicles considered, to obtain a single average acceleration signal. The Wavelet-based ODS magnitudes are obtained using this fleet-averaged acceleration signal. To test the repeatability for different fleets of vehicles, this process is conducted for three healthy bridge cases, as illustrated in Figure 10.

The results for the three vehicle fleets are broadly similar (with some minor variations), suggesting that variability between vehicle populations of this size (1000 vehicles) is minimal. Similar features can be observed to those present for the individual vehicle run considered in Figures 4–8 but with some notable differences: (i) the high-frequency zone (around 9–14 Hz) is more clearly defined for the results from a passing fleet of vehicles, and (ii) the zone around the

bridge first four natural frequencies is more intense for the fleet than for the single vehicle run with mean mass and velocity.

For the detection of scour-related stiffness losses, a damage indicator based on the difference between healthy and scoured fleet-averaged ODS magnitudes is proposed, as follows:

$$DI = FODS_{he} - FODS_{sc} \quad (8)$$

where $FODS_{he}$ and $FODS_{sc}$ represent the fleet-averaged wavelet-based ODS for healthy and scoured bridge conditions, respectively. An advantage of a damage indicator of this nature is that it presents the results in the spatial-frequency domain, which enables visualization of the scour effect in terms of the frequencies affected and their specific locations (thus facilitating scour-damage localization).

5.1. Detecting scour at a single location

In this section, scour is considered at one support of the multi-span bridge. Averaged bridge accelerations are obtained for fleets of 1000 traversing vehicles for the healthy and scoured bridge conditions by solving Eq. (5) and including sensor noise. Wavelet-based ODS magnitudes are derived from the averaged accelerations using the previously described procedure. Scour is modelled as a 25% loss of foundation stiffness at a specified bridge support.

Figure 11 depicts the differences in the fleet-averaged ODS (FODS) plots between the healthy and scoured bridges obtained from sensors located at each interior support, where scour is modelled at Support 2. Vertical dashed lines

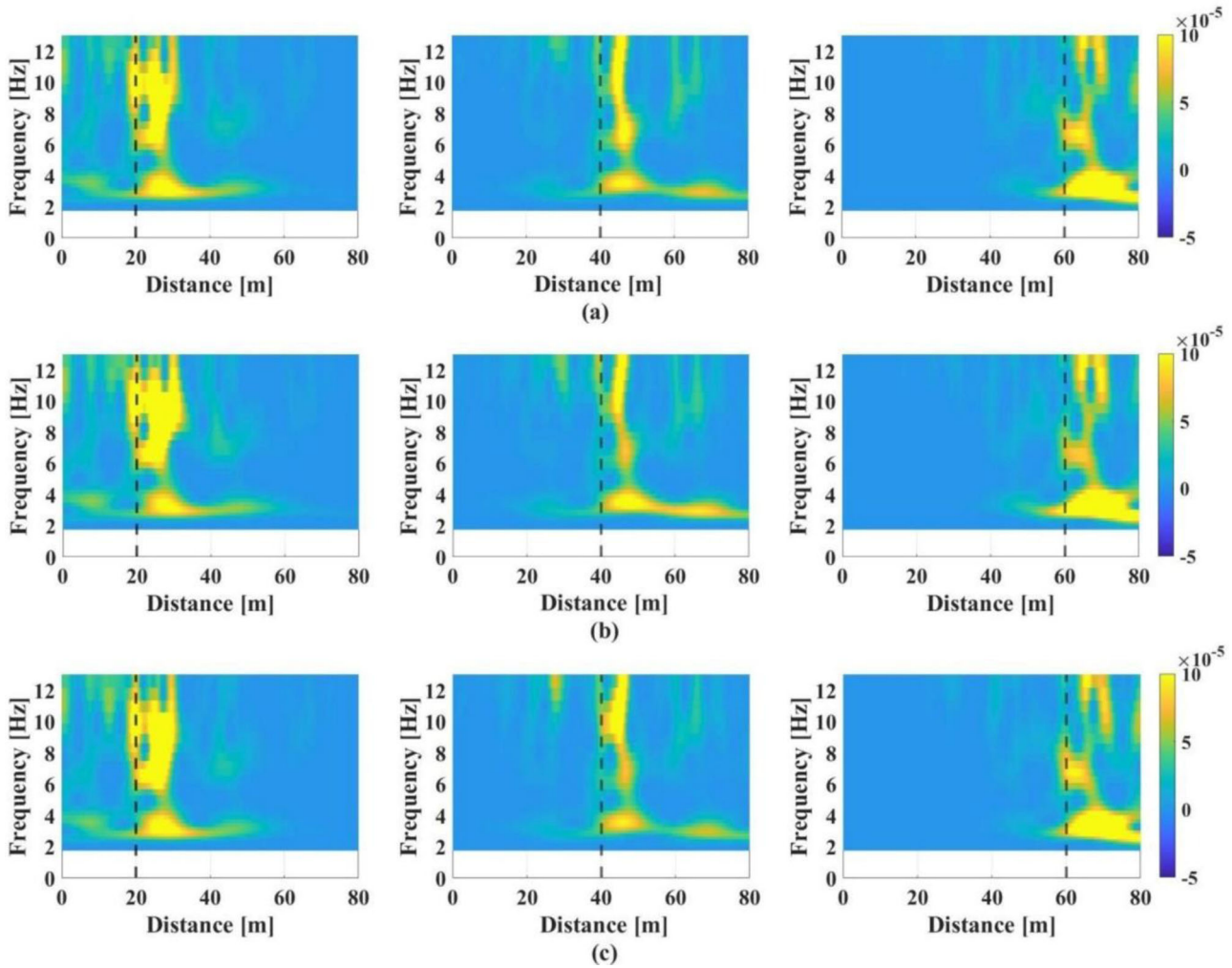


Figure 10. Examples of Wavelet-based ODS plots for healthy bridge condition using a fleet of vehicles: (a) first fleet; (b) second fleet; (c) third fleet. Vertical dashed line indicates the location of sensor in each plot.

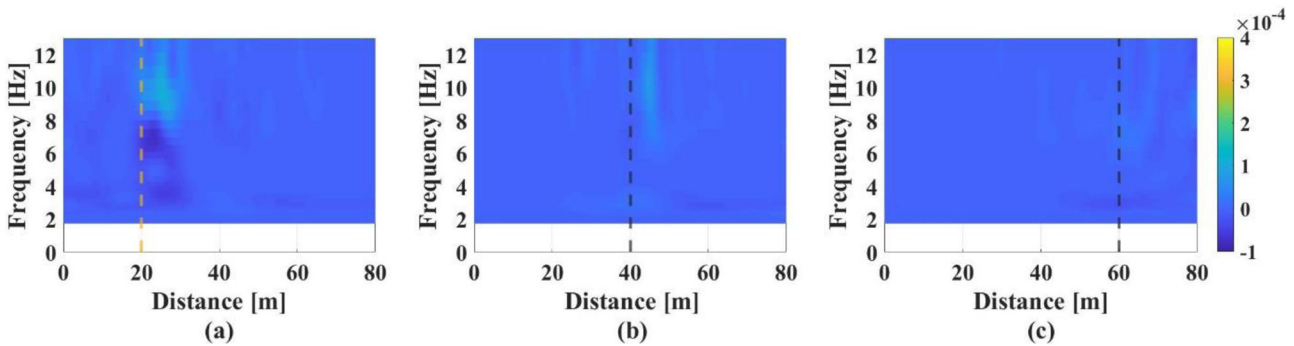


Figure 11. Differences between FODS for healthy and scoured bridge conditions (scour at Support 2) with sensor at: (a) Support 2; (b) Support 3; and (c) Support 4. Vertical dashed line indicates location of sensor (black = healthy support, orange = scoured support).

indicate the location of sensors at supports from which the data in each plot is derived. An orange dashed line indicates the scoured support. By observing each plot, significant intensity differences are only evident in Figure 11(a), i.e. from the data measured by the sensor at the location of scour.

Both positive and negative differences are apparent (dark and light colours), depending on the frequency, with positive values (healthy intensity > scoured intensity) occurring at higher frequencies and negative values

(healthy intensity < scoured intensity) occurring at both high and low frequencies. The results in Figure 11 suggest that by observation of the difference in the ODS measured at each sensor location, it is possible to identify which location is scoured. Similar results have also been found for scour at all other pier locations (not shown here), i.e. there are clearly visible differences in FODS intensity at piers where 25% stiffness loss has been simulated with minimal changes occurring at other (not scoured) locations.

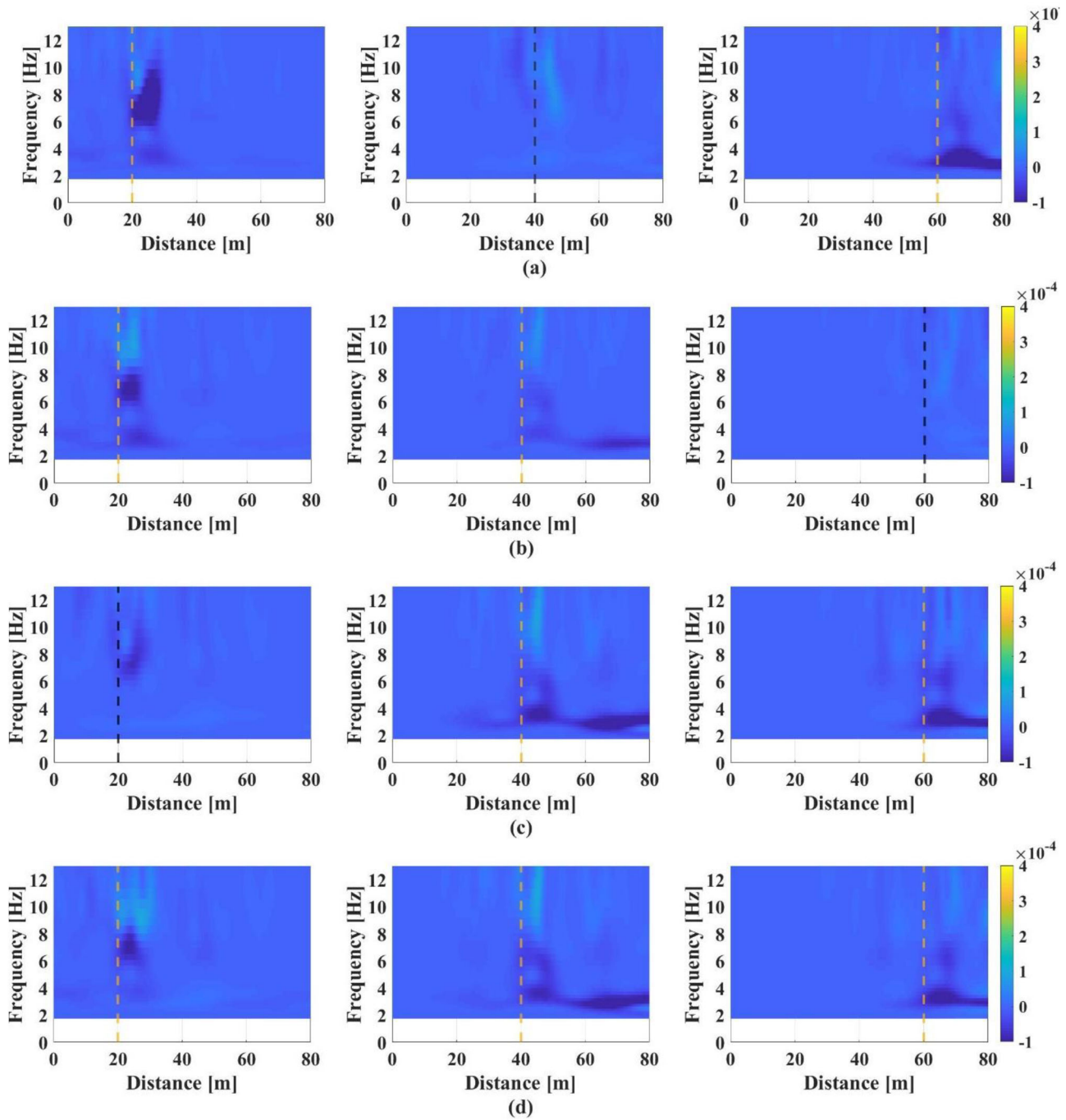


Figure 12. Differences between FODS for healthy and scoured bridge conditions for 25% stiffness loss at: (a) Supports 2 and 4; (b) Supports 2 and 3; (c) Supports 3 and 4; and (d) Supports 2, 3 and 4. Vertical dashed line indicates location of sensor (black = healthy support, orange = scoured support).

5.2. Detecting scour at multiple locations

When scour damage is present at multiple locations, the detection challenge is clearly greater. In this analysis, four scour cases equating to 25% stiffness loss are considered: (i) loss at each of supports 2 and 4; (ii) loss at each of supports 2 and 3; (iii) loss at each of supports 3 and 4; and (iv) loss at all three interior supports. The results for these four cases are presented in Figure 12. An additional analysis case is also carried out that considers just 15% stiffness loss at supports 2 and 4, while keeping the model and the statistical parameters similar to the previous analysis. The purpose of

this additional analysis is to assess the efficacy of the approach under smaller levels of scour damage, and the results are shown in Figure 13.

In Figure 12(a), where scour-related stiffness loss is simulated at Supports 2 and 4, significant dark coloured (negative intensity difference) zones can be seen for the sensors located at these two supports (left plot and right plot), with minimal intensity difference evident at the unscoured support (middle plot). Similarly, for the other cases of scour at two piers (Figure 12b and 12c), there are significant FODS differences for the sensors at the scour locations and little difference for the other sensors. In Figure 12(b), scour

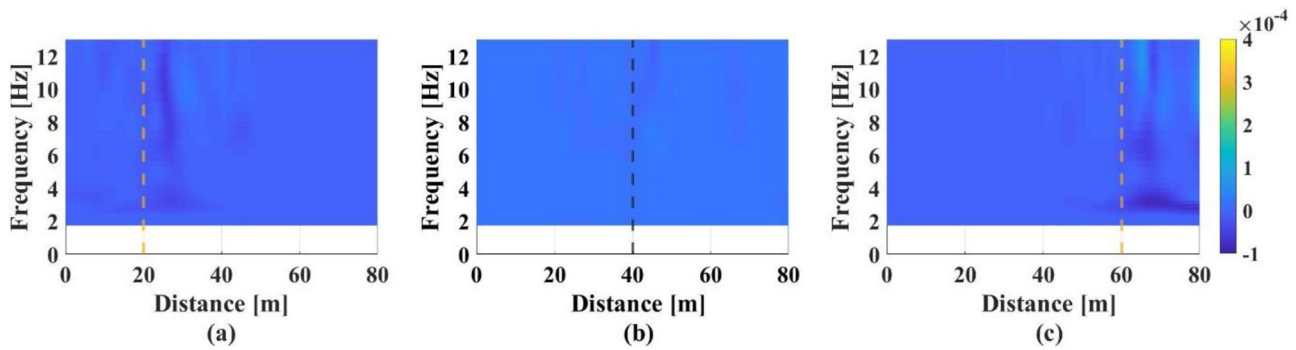


Figure 13. Differences between FODS for healthy and 15% scour-related stiffness loss (scour at Supports 2 and 4) with sensor at: (a) Support 2; (b) Support 3; and (c) Support 4. Vertical dashed line indicates location of sensor (black = healthy support, orange = scoured support).

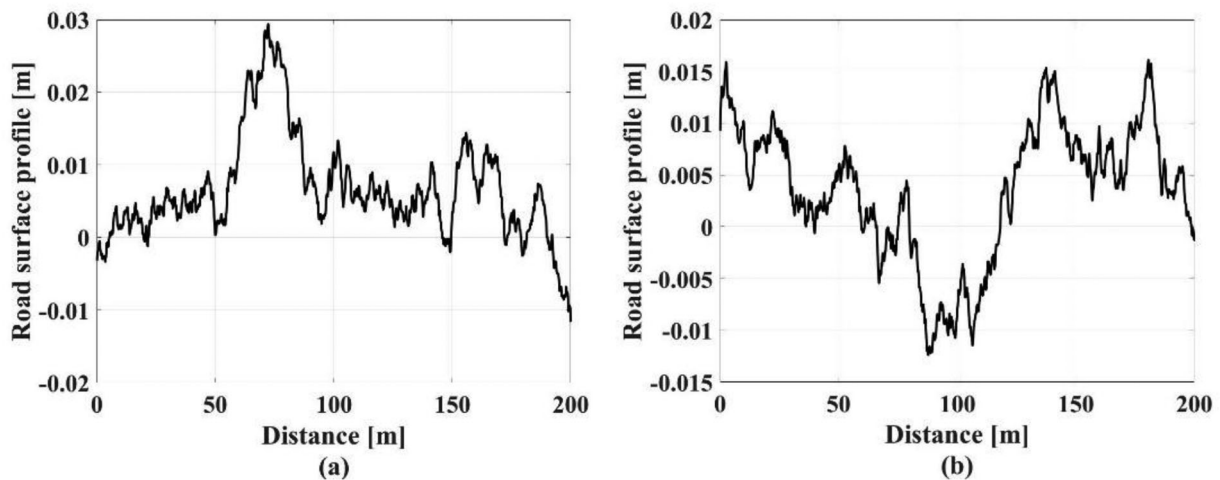


Figure 14. Road surface profiles (Class A): (a) profile 1—used in previous analysis; (b) profile 2.

occurs at Supports 2 and 3 and a difference in intensity can be observed at the sensors located at these points (left and middle plots). In Figure 12(c), scour occurs at Supports 3 and 4, and again intensity difference can be observed at these sensor locations (middle and right plots).

Where scour is located at all three piers, Figure 12(d), there are dark coloured zones in the FODS plots from the sensors at all three pier locations. Similar results are seen in Figure 13, which corresponds to 15% scour stiffness loss at supports 2 and 4, suggesting that the proposed approach is also effective under this lower level of scour damage. While the interpretation of the results involves a level of subjectivity, the damage indicator would appear to provide good visual evidence for both the presence and location of pier stiffness loss as a result of simulated scour at various locations.

5.3. Influence of road surface profile

Road surface roughness has a significant influence on bridge accelerations and may affect the success of vibration-based damage detection approaches. The traversing vehicles interact with the bridge through the road profile and any change in the profile amplitude alters vehicle and bridge acceleration amplitudes. The damage detection approach proposed in this paper is assessed here in the presence of a changing road profile. The FODS analysis is repeated using

completely different, Class ‘A’ randomly generated road profiles for the healthy and scoured bridge conditions—see Figure 14—all other parameters remaining unchanged. The FODS results are shown in Figure 15.

It can be seen in the figure that the scour damage manifests itself as a change in the magnitude of the FODS differences near the scoured locations, despite a significant change in the road surface profile. The dark spots in the plots for sensors at supports 2 and 4 are visible in Figure 15, confirming the detection of scour when the road profile has changed. This brief analysis suggests that the approach is not strongly sensitive to changes in the road surface profile itself. However, only Class ‘A’ profiles have been considered, often presented as being typical of a well-maintained highway.

5.4. Influence of span length

Dynamic amplification in bridges is strongly influenced by frequency matching, i.e. a resonance effect between bridge natural frequencies and the pseudo-frequencies related to the moving vehicle which derive from its speed relative to bridge length. To confirm the consistency of results, the FODS analysis is repeated in this section for another 4-span bridge, this time with four spans of length 10 m. All other parameters were maintained as before. Two cases of scour-related stiffness loss are considered: (i) 25% loss at supports

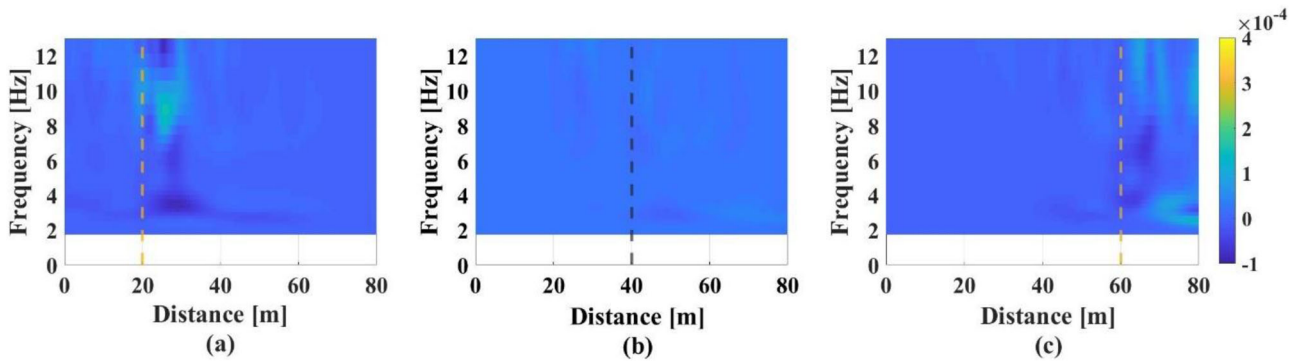


Figure 15. Differences between FODS for healthy and 25% scoured bridge (scour at Supports 2 and 4) and different road profile conditions with sensor at: (a) Support 2; (b) Support 3; and (c) Support 4. Vertical dashed line indicates location of sensor (black = healthy support, orange = scoured support).

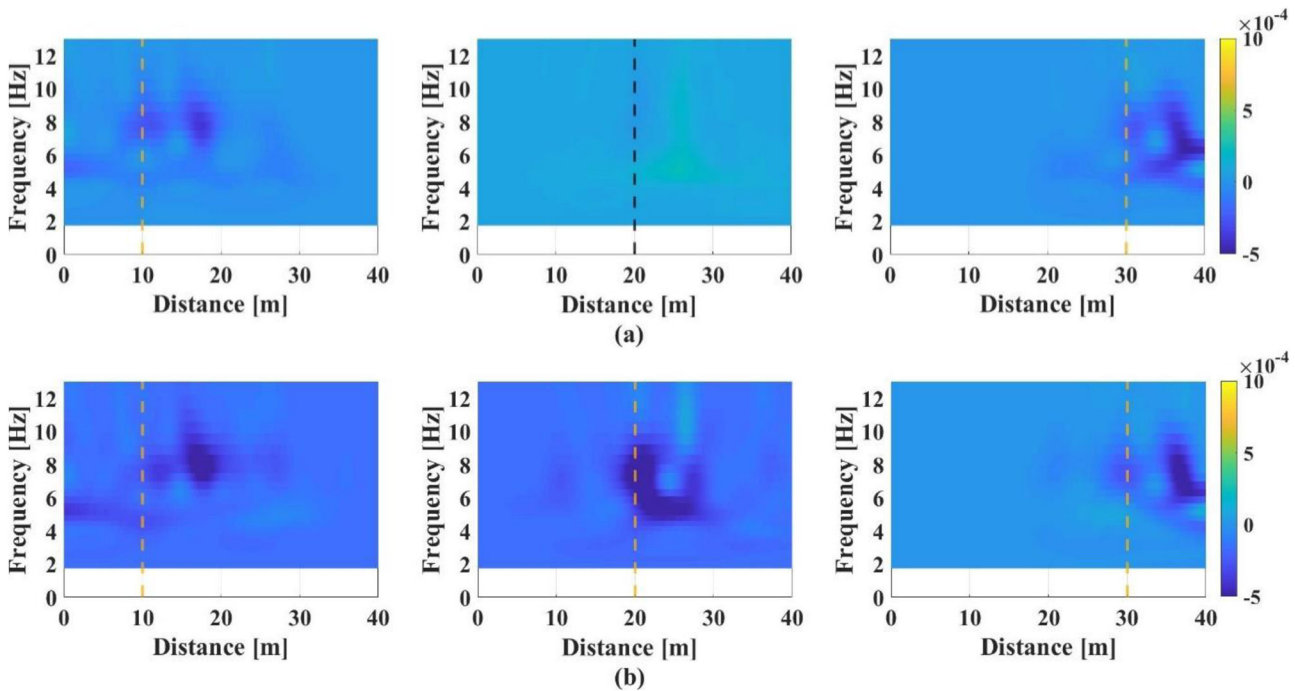


Figure 16. Differences between FODS for healthy and scoured bridge conditions for scour at: (a) Supports 2 and 4 and (b) Supports 2, 3 and 4. Vertical dashed line indicates location of sensor (black = healthy support, orange = scoured support).

2 and 4 and (ii) 25% loss at all three interior supports. The FODS results are presented in Figure 16.

In Figure 12(a), it can be seen that intensity differences are evident at the location of the scoured supports as detected by the sensors at these locations (supports 2 and 4). Similarly, in Figure 12(b), differences can be observed in the sensor data measured at all three scoured supports. While the pattern of the differences is not the same as for the $4 \times 20\text{m}$ bridge analysed previously, the conclusion is the same as before, namely, that there are significant negative differences obtained by analysis of the data from sensors located at the supports where scour damage has been simulated to have occurred. Although the differences in ODS for detecting scour are small in magnitude, the simulations suggest that these differences can be detected using the proposed statistical approach. There is repeatability of the results despite the changing vehicles, road surface, noise, and bridge geometrical conditions in the numerical study.

6. Conclusions

This paper proposes a novel statistical approach using wavelet-derived ODS for detecting the location of bridge scour at multiple foundations. Scour location detection, with the possibility of multiple locations at one time, has always been challenging for the contemporary vibration-based scour monitoring techniques. A structure's ODS contain valuable information relating to the structural condition and are sensitive to global structural changes, including changes to boundary conditions such as support stiffness. A wavelet-based ODS approach using a statistical simulated bridge acceleration response is numerically demonstrated in this paper using a bridge model consisting of multiple simply supported spans, with sprung piers resting on damped foundations.

A population of vehicles is used to derive average bridge accelerations at supports and ODS are calculated using the

auto-power spectrum of the wavelet coefficients of the derived acceleration signal. The difference in wavelet-derived ODS is considered as a scour damage indicator, which is observed to be an improvement on previous methods as it does not rely on detecting changes in single mode shapes or frequencies (difficult when closely-spaced), rather it enables detection of scour over a range of frequencies thus minimising the information required by an asset manager. The main advantage of using the Wavelet transform is that it provides results in both the frequency and spatial domains, which enables the identification of scour location.

Use of wavelet-derived ODS is shown to be potentially capable of detecting scour-related stiffness losses at multiple supports without the need for accurate modal information from the structure, i.e. it is not reliant on detecting small changes in individual frequencies or mode shapes. Instead, the wavelet-derived ODS provide information on changes over a range of operational frequencies thus minimizing the requirement for highly accurate modal information. A statistical approach overcomes the challenges of variable vehicle velocity and mass, which can adversely influence bridge accelerations for SHM techniques. The proposed approach has shown promising results in the numerical simulations and is found to be effective in detecting scour-related stiffness losses at individual and multiple supports of the bridge.

The paper provides a theoretical concept and numerical validation for scour location detection. However, a full-scale real-life demonstration of the approach is recommended as part of future work to test the resilience of the approach on real-life bridges where environmental variations and other physical phenomena might limit the effectiveness. Also, future studies are planned to determine if the proposed method can be extended to detect abutment scour.

Acknowledgements

The authors wish to acknowledge the financial support received from Science Foundation Ireland (SFI) under the US-Ireland R&D partnership with the National Science Foundation (NSF) and Invest Northern Ireland (ID: 16/US/13277). We also acknowledge the FHWA for access to the Long-Term Pavement Performance (LTPP) WIM data.

Disclosure statement

No potential conflict of interest was reported by the authors.

ORCID

Eugene J. O'Brien  <http://orcid.org/0000-0002-6867-1009>
 Daniel P. McCrum  <http://orcid.org/0000-0002-4367-1627>
 Muhammad Arslan Khan  <http://orcid.org/0000-0002-2930-7685>
 Luke J. Prendergast  <http://orcid.org/0000-0003-3755-0391>

References

- Adhikary, S., Singh, Y., & Paul, D. (2014). Modelling of soil-foundation-structure system. *Soil Dynamics and Earthquake Engineering*, 61–62, 13–28. doi:10.1016/j.soildyn.2014.01.017
- Asnaashari, E., & Sinha, J. K. (2014). Development of residual operational deflection shape for crack detection in structures. *Mechanical Systems and Signal Processing*, 43(1–2), 113–123. doi:10.1016/j.ymsp.2013.10.003
- Bai, R. B., Song, X. G., Radziński, M., Cao, M. S., Ostachowicz, W., & Wang, S. S. (2014). Crack location in beams by data fusion of fractal dimension features of laser-measured operating deflection shapes. *Smart Structures and Systems*, 13(6), 975–991. doi:10.12989/sss.2014.13.6.975
- Bao, T., & Liu, Z. (2017). Vibration-based bridge scour detection: a review. *Structural Control and Health Monitoring*, 24(7), e1937. doi:10.1002/stc.1937
- Bao, T., & Liu, Z. L. (2020). Evaluation of Winkler model and Pasternak model for dynamic soil-structure interaction analysis of structures partially embedded in soils. *International Journal of Geomechanics*, 20(2), 04019167. doi:10.1061/(ASCE)GM.1943-5622.0001519
- Bao, T., Liu, Z. L., & Bird, K. (2019). Influence of soil characteristics on natural frequency-based bridge scour detection. *Journal of Sound and Vibration*, 446, 195–210. doi:10.1016/j.jsv.2019.01.040
- Bao, T., Swartz, R. A., Vitton, S., Sun, Y., Zhang, C., & Liu, Z. (2017). Critical insights for advanced bridge scour detection using the natural frequency. *Journal of Sound and Vibration*, 386, 116–133. doi:10.1016/j.jsv.2016.06.039
- Buckley, T., Watson, P., Cahill, P., Jaksic, V., & Pakrashi, V. (2018). Mitigating the structural vibrations of wind turbines using tuned liquid column damper considering soil-structure interaction. *Renewable Energy*, 120, 322–341. doi:10.1016/j.renene.2017.12.090
- Cantero, D., O'Brien, E. J., & González, A. (2010). Modelling the vehicle in vehicle-infrastructure dynamic interaction studies. *Proceedings of the Institution of Mechanical Engineers, Part K: Journal of Multi-Body Dynamics*, 224(2), 243–248. doi:10.1243/14644193JMBD228
- Cao, M., Zhu, X., Xu, W., Li, X., Xu, H., & Manoach, E. (2017). Detection of debonding in steel-reinforced bridges using wavelet curvature features of laser-measured operating deflection shapes. *Journal of Vibroengineering*, 19(3), 1845–1853. doi:10.21595/jve.2017.18534
- Cebon, D. (1999). *Handbook of vehicle-road interaction*. Lisse, The Netherlands: Swets and Zeitlinger.
- Chortis, G., Askarinejad, A., Prendergast, L., Li, Q., & Gavin, K. (2020). Influence of scour depth and type on p-y curves for monopiles in sand under monotonic lateral loading in a geotechnical centrifuge. *Ocean Engineering*, 197, 106838. doi:10.1016/j.oceaneng.2019.106838
- de Siqueira, L. P., & Nogueira, F. (2001). Application of modal analysis and operating deflection shapes on the study of trucks and buses dynamic behavior. *SAE Transactions*, 110(2), 418–424.
- Elsaid, A., & Seracino, R. (2014). Rapid assessment of foundation scour using the dynamic features of bridge superstructure. *Construction and Building Materials*, 50, 42–49. doi:10.1016/j.conbuildmat.2013.08.079
- Fisher, M., Chowdhury, M. N., Khan, A. A., & Atamturktur, S. (2013). An evaluation of scour measurement devices. *Flow Measurement and Instrumentation*, 33, 55–67. doi:10.1016/j.flowmeasinst.2013.05.001
- Fitzgerald, P. C., Malekjafarian, A., Bhowmik, B., Prendergast, L. J., Cahill, P., Kim, C.-W., ... O'Brien, E. J. (2019a). Scour damage detection and structural health monitoring of a laboratory-scaled bridge using a vibration energy harvesting device. *Sensors*, 19(11), 2572. doi:10.3390/s19112572
- Fitzgerald, P. C., Malekjafarian, A., Cantero, D., O'Brien, E. J., & Prendergast, L. J. (2019b). Drive-by scour monitoring of railway bridges using a wavelet-based approach. *Engineering Structures*, 191, 1–11. doi:10.1016/j.engstruct.2019.04.046
- Foti, S., & Sabia, D. (2011). Influence of foundation scour on the dynamic response of an existing bridge. *Journal of Bridge Engineering*, 16(2), 295–304. doi:10.1061/(ASCE)BE.1943-5592.0000146
- Gade, S., Schlombs, R., Hundecck, C., & Fenselau, C. (2009). *Operational modal analysis on a wind turbine gearbox*. Conference & Exposition on Structural Dynamics, 1–11.

- Giordano, P. F., Prendergast, L., & Limongelli, M. (2020). A framework for assessing the value of information for health monitoring of scoured bridges. *Journal of Civil Structural Health Monitoring*, 10(3), 485–496. doi:10.1007/s13349-020-00398-0
- González, A. (2010). Vehicle-bridge dynamic interaction using finite element modelling. In *Finite element analysis*. Rijeka, Croatia: InTech.
- Hamill, L. (1999). *Bridge hydraulics*. London: E and FN Spon.
- Hera, A., & Hou, Z. (2004). Application of wavelet approach for ASCE structural health monitoring benchmark studies. *Journal of Engineering Mechanics*, 130(1), 96–104. doi:10.1061/(ASCE)0733-9399(2004)130:1(96)
- Hou, Z., Noori, M., & Amand, R. S. (2000). Wavelet-based approach for structural damage detection. *Journal of Engineering Mechanics*, 126(7), 677–683. doi:10.1061/(ASCE)0733-9399(2000)126:7(677)
- ISO. (1995). Mechanical vibration—Road surface profiles—Reporting of measured data.
- Ju, S.-H. (2013). Determination of scoured bridge natural frequencies with soil–structure interaction. *Soil Dynamics and Earthquake Engineering*, 55, 247–254. doi:10.1016/j.soildyn.2013.09.015
- Keenahan, J., O'Brien, E. J., McGetrick, P. J., & Gonzalez, A. (2014). The use of a dynamic truck–trailer drive-by system to monitor bridge damping. *Structural Health Monitoring*, 13(2), 143–157. doi:10.1177/1475921713513974
- Khan, M. A., McCrum, D. P., Prendergast, L. J., O'Brien, E. J., Fitzgerald, P. C., & Kim, C.-W. (2021). Laboratory investigation of a bridge scour monitoring method using decentralized modal analysis. *Structural Health Monitoring*, 20, 1475921720985122.
- Klinga, J. V., & Alipour, A. (2015). Assessment of structural integrity of bridges under extreme scour conditions. *Engineering Structures*, 82, 55–71. doi:10.1016/j.engstruct.2014.07.021
- Kong, X., & Cai, C. (2016). Scour effect on bridge and vehicle responses under bridge–vehicle–wave interaction. *Journal of Bridge Engineering*, 21(4), 04015083. doi:10.1061/(ASCE)BE.1943-5592.0000868
- Kwon, Y. W., & Bang, H. (2000). *The finite element method using MATLAB*. Boca Raton, FL: CRC Press.
- Lagasse, P., Schall, J., Johnson, F., Richardson, E., & Chang, F. (1995). Stream Stability at Highway Structures: Federal Highway Administration Hydraulic Engineering Circular No. 20. Publication FHWA-IP-90-014.
- Li, Q., Prendergast, L., Askarinejad, A., Chortis, G., & Gavin, K. (2020). Centrifuge modeling of the impact of local and global scour erosion on the monotonic lateral response of a monopile in sand. *Geotechnical Testing Journal*, 43(5), 20180322. doi:10.1520/GTJ20180322
- Maddison, B. (2012). Scour failure of bridges. *Proceedings of ICE - Forensic Engineering*, 165, 14.
- Malekjafarian, A., Kim, C.-W., O'Brien, E. J., Prendergast, L. J., Fitzgerald, P. C., & Nakajima, S. (2020). Experimental demonstration of a mode shape-based scour monitoring method for multi-span bridges with shallow foundations. *Journal of Bridge Engineering*, 25(8), 04020050. doi:10.1061/(ASCE)BE.1943-5592.0001586
- McGetrick, P. J., & Kim, C. W. (2013). A parametric study of a drive by bridge inspection system based on the Morlet wavelet. *Key Engineering Materials*, 569–570, 262–269. doi:10.4028/www.scientific.net/KEM.569-570.262
- McGetrick, P., & Kim, C. (2014). *A wavelet based drive-by bridge inspection system*. Proceedings of the 7th International Conference on Bridge Maintenance Safety and Management (IABMAS'14).
- Melville, B. W., & Coleman, S. E. (2000). *Bridge scour*. Colorado, USA: Water Resources Publication.
- Mızrak, C., & Esen, I. (2015). Determining effects of wagon mass and vehicle velocity on vertical vibrations of a rail vehicle moving with a constant acceleration on a bridge using experimental and numerical methods. *Shock and Vibration*, 2015, 1–15. doi:10.1155/2015/183450
- Mylonakis, G., Nikolaou, S., & Gazetas, G. (2006). Footings under seismic loading: Analysis and design issues with emphasis on bridge foundations. *Soil Dynamics and Earthquake Engineering*, 26(9), 824–853. doi:10.1016/j.soildyn.2005.12.005
- O'Brien, E. J., Heitner, B., Žnidarič, A., Schoefs, F., Causse, G., & Yalamas, T. (2020). Validation of bridge health monitoring system using temperature as a proxy for damage. *Structural Control and Health Monitoring*, 27(9), e2588. doi:10.1002/stc.2588
- O'Brien, E., Khan, M. A., McCrum, D., & Žnidarič, A. (2020). Using statistical analysis of an acceleration-based bridge weigh-in-motion system for damage detection. *Applied Sciences*, 10(2), 663. doi:10.3390/app10020663
- Oztoprak, S., & Bolton, M. (2013). Stiffness of sands through a laboratory test database. *Géotechnique*, 63(1), 54–70. doi:10.1680/geot.10.P.078
- Pais, A., & Kausel, E. (1988). Approximate formulas for dynamic stiffnesses of rigid foundations. *Soil Dynamics and Earthquake Engineering*, 7(4), 213–227. doi:10.1016/S0267-7261(88)80005-8
- Prendergast, L. J., & Gavin, K. (2014). A review of bridge scour monitoring techniques. *Journal of Rock Mechanics and Geotechnical Engineering*, 6(2), 138–149. doi:10.1016/j.jrmge.2014.01.007
- Prendergast, L. J., & Gavin, K. (2016). A comparison of initial stiffness formulations for small-strain soil–pile dynamic Winkler modelling. *Soil Dynamics and Earthquake Engineering*, 81, 27–41. doi:10.1016/j.soildyn.2015.11.006
- Prendergast, L. J., Gavin, K., & Hester, D. (2017). Isolating the location of scour-induced stiffness loss in bridges using local modal behaviour. *Journal of Civil Structural Health Monitoring*, 7(4), 483–503. doi:10.1007/s13349-017-0238-3
- Prendergast, L. J., Hester, D., & Gavin, K. (2016a). Determining the presence of scour around bridge foundations using vehicle-induced vibrations. *Journal of Bridge Engineering*, 21(10), 04016065. doi:10.1061/(ASCE)BE.1943-5592.0000931
- Prendergast, L. J., Hester, D., & Gavin, K. (2016b). Development of a vehicle-bridge-soil dynamic interaction model for scour damage modelling. *Shock and Vibration*, 2016, 1–15. doi:10.1155/2016/7871089
- Prendergast, L. J., Hester, D., Gavin, K., & O'sullivan, J. (2013). An investigation of the changes in the natural frequency of a pile affected by scour. *Journal of Sound and Vibration*, 332(25), 6685–6702. doi:10.1016/j.jsv.2013.08.020
- Reilly, T. (2011). A review of signal processing and analysis tools for comprehensive rotating machinery diagnostics. In *Rotating machinery, structural health monitoring, shock and vibration* (Vol. 5). New York, USA: Springer.
- Richardson, M. H. (1997). Is it a mode shape, or an operating deflection shape? *SV Sound and Vibration*, 31(1), 54–61.
- Schwarz, B., McHargue, P., & Richardson, M. (2019). ODS & modal testing using a transmissibility chain. In *Special Topics in Structural Dynamics* (Vol. 5). Cham, Switzerland: Springer.
- Schwarz, B. J., & Richardson, M. H. (1999). Introduction to operating deflection shapes. *CSI Reliability Week*, 10, 121–126.
- Schwarz, B., & Richardson, M. (2004). *Measurements required for displaying operating deflection shapes*. Presented at IMAC XXII, January 26, 29.
- Sekiya, H., Kubota, K., & Miki, C. (2017). Simplified portable bridge weigh-in-motion system using accelerometers. *Journal of Bridge Engineering*, 23(1), 04017124. doi:10.1061/(ASCE)BE.1943-5592.0001174
- Shirgir, V., Ghanbari, A., & Shahrouzi, M. (2016). Natural frequency of single pier bridges considering soil–structure interaction. *Journal of Earthquake Engineering*, 20(4), 611–632. doi:10.1080/13632469.2015.1104754
- Taha, M. R., Noureldin, A., Lucero, J., & Baca, T. (2006). Wavelet transform for structural health monitoring: a compendium of uses and features. *Structural Health Monitoring*, 5(3), 267–295. doi:10.1177/1475921706067741
- Tedesco, J., McDougal, W. G., & Ross, C. A. (2000). *Structural dynamics*. New York, USA: Pearson Education.
- Teolis, A., & Benedetto, J. J. (1998). *Computational signal processing with wavelets*. Boston, USA: Springer.

- Tyan, F., Hong, Y.-F., Tu, S.-H., & Jeng, W. S. (2009). Generation of random road profiles. *Journal of Advanced Engineering*, 4(2), 1373–1378.
- Vold, H., Schwarz, B., & Richardson, M. (2000). *Measuring operating deflection shapes under non-stationary conditions*. 18th International Modal Analysis Conference, San Antonio, Texas.
- Walker, D., & Cebon, D. (2012). *The metamorphosis of LTPP traffic data*. 6th International Conference on Weigh-In-Motion (ICWIM 6) International Society for Weigh-In-Motion, Dallas, TX.
- Walker, D., Selezneva, O., & Wolf, D. (2012). *Findings from LTPP SPS WIM systems validation study*. 6th International Conference on Weigh-In-Motion (ICWIM 6) International Society for Weigh-In-Motion, Dallas, TX.
- Wardhana, K., & Hadipriono, F. C. (2003). Analysis of recent bridge failures in the United States. *Journal of Performance of Constructed Facilities*, 17(3), 144–150. doi:10.1061/(ASCE)0887-3828(2003)17:3(144)
- Xiang, J.-W., Matsumoto, T., Long, J.-Q., & Ma, G. (2013). Identification of damage locations based on operating deflection shape. *Nondestructive Testing and Evaluation*, 28(2), 166–180. doi: 10.1080/10589759.2012.716437
- Xiong, W., Kong, B., Tang, P., & Ye, J. (2018). Vibration-based identification for the presence of scouring of cable-stayed bridges. *Journal of Aerospace Engineering*, 31(2), 04018007. doi:10.1061/(ASCE)AS.1943-5525.0000826
- Xu, W., Radziński, M., Ostachowicz, W., & Cao, M. (2013). Damage detection in plates using two-dimensional directional Gaussian wavelets and laser scanned operating deflection shapes. *Structural Health Monitoring*, 12(5–6), 457–468. doi:10.1177/1475921713492365
- Yoon, M. K., Heider, D., Gillespie, J. W., Ratcliffe, C. P., & Crane, R. M. (2010). Local damage detection with the global fitting method using operating deflection shape data. *Journal of Nondestructive Evaluation*, 29(1), 25–37. doi:10.1007/s10921-010-0062-8
- Zhang, C., Li, B., Yang, Z., Xiao, W., & He, Z. (2013a). Crack location identification of rotating rotor systems using operating deflection shape data. *Science China Technological Sciences*, 56(7), 1723–1732. doi:10.1007/s11431-013-5243-0
- Zhang, Y., Lie, S. T., & Xiang, Z. (2013b). Damage detection method based on operating deflection shape curvature extracted from dynamic response of a passing vehicle. *Mechanical Systems and Signal Processing*, 35(1–2), 238–254. doi:10.1016/j.ymsp.2012.10.002
- Zhu, X., & Law, S. (2006). Wavelet-based crack identification of bridge beam from operational deflection time history. *International Journal of Solids and Structures*, 43(7–8), 2299–2317. doi:10.1016/j.ijsolstr.2005.07.024

Appendix A

Table A1. The absolute frequencies for a range of scour cases and modes of vibration (for the data shown in Figure 3).

Healthy/Hz	25% A1	45% A1	25% P1	45% P1	25% P2	45% P2	25% P3	45% P3	25% A3	45% A3
3.81	3.80	3.79	3.75	3.64	3.74	3.62	3.76	3.64	3.81	3.79
3.93	3.92	3.89	3.90	3.88	3.93	3.93	3.90	3.88	3.92	3.89
4.10	4.08	4.06	4.10	4.10	4.08	4.05	4.10	4.10	4.08	4.06
4.26	4.25	4.25	4.26	4.26	4.26	4.26	4.26	4.26	4.25	4.25
9.51	9.41	8.99	9.01	8.27	8.95	8.22	9.04	8.31	9.42	8.99
10.29	10.06	9.77	10.00	9.92	10.28	10.28	10.00	9.90	10.05	9.75
11.46	11.12	10.83	11.40	11.36	11.05	10.83	11.39	11.36	11.12	10.83
12.95	12.40	12.14	12.80	12.69	12.94	12.95	12.80	12.68	12.41	12.16
13.47	13.32	13.29	13.33	13.28	13.33	13.26	13.33	13.28	13.32	13.29